12-2019

Comparative Study of Winding Configurations of a Five-Phase Flux-Switching PM Machine

Hao Chen

Xiangdong Liu

Ayman M. EL-Refaie

Jing Zhao

Nabeel Demerdash

See next page for additional authors

Authors
Hao Chen, Xiangdong Liu, Ayman M. EL-Refaie, Jing Zhao, Nabeel Demerdash, and Jiangbiao He

Comparative Study of Winding Configurations of a Five-Phase Flux-Switching PM Machine

Hao Chen
School of Automation, Beijing Institute of Technology, Beijing, China
Xiangdong Liu
School of Automation, Beijing Institute of Technology, Beijing, China
Ayman M. EL-Refaie
Department of Electrical and Computer Engineering, Marquette University, Milwaukee, WI
Jing Zhao
School of Automation, Beijing Institute of Technology, Beijing, China
Nabeel A. O. Demerdash
Department of Electrical and Computer Engineering, Marquette University, Milwaukee, WI
Jiangbiao He
Department of Electrical and Computer Engineering, University of Kentucky, Lexington, KY

Abstract:

This paper introduces a general method for determination of the most suitable winding configurations for five-phase flux-switching permanent magnet (FSPM) machines, associated with feasible stator/rotor-pole combinations. Consequently, the effect of winding configurations on the performance of a five-phase outer-rotor FSPM machine is thoroughly investigated, including non-overlapping concentrated windings (single-layer, double-layer, and multi-layer) as well as distributed winding. The electromagnetic characteristics in the low-speed region, the flux-weakening capability in the high-speed region, and the fault-tolerant capability under faulty situations are evaluated and compared in detail. This work shows that compared with the conventional single-layer or double-layer concentrated windings, the FSPM machine with multi-layer type winding exhibits lower torque ripple and losses. Meanwhile, the motor with distributed windings possesses higher torque density and larger inductance. Finally, a prototype is manufactured, and the analysis results are validated by experiments.

Keywords

Windings, Stator windings, Traction motors, Torque, Rotors, Brushless motors

SECTION I. Introduction

With the increasing concerns on environmental protection and energy security, electric vehicles (EVs) have been widely recognized as a promising candidate to offer an ultimate solution for clean-energy personal mobility [1], [2]. By placing motors in the wheels, the advantages of flexibility and simplicity make the in-wheel traction preferable for EV applications [3].

Instead of conventional permanent magnet (PM) brushless motors with surface-mounted or interior PMs on the rotor, stator-PM machines have attracted considerable attention in this application due to their robust and simple rotor, as well as their favorable PM thermal dissipation [4], [5]. Among the stator-PM motors, flux-switching PM (FSPM) machines exhibit higher torque capability and power density than doubly-salient and flux-reversal PM machines due to the flux-concentration effect [4]. Recently, various topologies have been introduced for FSPM machines, including original [6], hybrid excited [7], partitioned stator [8], and multi-tooth FSPM machines [9], etc. However, most of these machines are limited to normal three-phase inner-rotor system, even though the multi-phase (>3) motors have exhibited better fault-tolerant capabilities and lower torque ripples [10], [11]. Moreover, outer-rotor motors are desirable for in-wheel traction applications because of their low audible noise, compact constructions, and high transmission efficiency with gearless operation [12]. Accordingly, a five-phase outer-rotor FSPM machine is analyzed and investigated in this paper.

The traditional FSPM machine comprises a robust rotor which is identical to that of switched reluctance motors, and a rather complex stator. The stator contains laminated “U”-shaped segments, between which circumferentially magnetized magnets are sandwiched with alternative opposite polarity, over which the “U”-shaped segments are wound by fractional-slot concentrated windings (FSCWs) [13]. FSCW PM motors have been gaining interest as a result of serval advantages, including high-power density, high efficiency, short end turns, and high slot fill factor [14]. However, FSPM machines with FSCWs suffer from high losses by the ill-influence of the presence of both sub- and super-harmonic components in the stator magnetomotive force (MMF). In order to reduce the stator MMF harmonics, reference [15] proposed a method by increasing the number of layers in the stator winding. Consequently, the effects of number of layers on performance of interior PM motors were investigated in [16] and [17]. These investigations indicated that by going to higher number of layers, the efficiency, especially in the high-speed region, and the torque density are significantly improved. Multi-layer

windings have been implemented in FSPM machines with 12/11 stator/rotor-pole [18] and 12/13-pole [19], respectively. These works show that compared with the conventional double-layer configuration, the motors with four-layer windings have lower losses and lower torque ripples. On the other hand, FSPM machines have not been limited to concentrated windings. In [20] and [21], 6/14-pole and 24/16-pole FSPM machines with distributed windings were introduced, and proved that the FSPM machines with distributed windings have higher torque density than their concentrated winding counterparts. A 12/7-pole FSPM machine with full-pitched distributed winding is discussed in [22] and [23], this machine shows lower cogging torque and larger inductance compared with the conventional 12/10-pole FSPM concentrated winding machine. New winding configuration possibilities have been attempted for FSPM machines [24]–[25][26]. However, the prior literatures mostly focus on few stator/rotor-pole combinations. A general method to determine the winding configuration of FSPM machines still is lacking. In addition, comprehensive comparisons between these various winding configurations have not been made.

This paper presents new contributions to the specific subject by comparing the performances of FSPM machines with different winding configurations, i.e., both concentrated windings (single-layer, double-layer, and multi-layer) and distributed wingdings. The overall performances are evaluated including the electromagnetic characteristics in the low-speed region, the flux-weakening capability in the high-speed region, and the fault-tolerant capability under faulty situations. Other new aspects of interest are the determination of the most suitable winding configuration for the five-phase FSPM machine, associated with feasible stator/rotor-pole combinations, novel multi-layer winding topologies for FSPM machines, and the concept of spokes per phase for FSPM machines which is different from other methods previously presented in literature [29] as will be discussed later. Also, the analysis is supported by experimental results.

SECTION II. Design of Balanced Symmetrical Windings

For an m-phase FSPM machine with balanced and symmetrical windings, based on the “magnetic gear effect”, the relationship between the PM pole-pair number, P_{pm}, the armature winding pole-pair number, P_{aw}, and the number of rotor poles, N_r, is as follows [27]:

$$\begin{aligned} P_{pm} + P_{aw} &= N_r \\ P_{pm} &= N_s/2 \end{aligned} \quad (1)(2)$$

where, N_s is the number of stator poles (teeth). It should be noted that the number, N_s, must be even, and the number, N_r, in FSPM machines is equivalent to the number of pole pairs rather than poles in conventional rotor-PM machines. In addition, such machines exhibit potential unbalanced magnetic force (UMF) when Nr is an odd number. In these machines, the machine periodicity, τ, is defined as,

$$\tau = GCD(N_s \cdot k_l/2, P_{aw}) \quad (3)$$

where, GCD is greatest common divisor, $k_l = 1$ for a single-layer winding, while $k_l = 2$ for a double-layer winding. The star of slots in one basic repeating unit (an equivalent machine with the least slots and poles) is characterized by $[N_s \cdot k_l/(2\tau)]$ spokes, in which each spoke contains τ phasors. Hence, the feasible combination of N_s and N_r should satisfy,

$$N_s/2\tau = mk, \text{where } k = 1,2, \ldots \quad (4)$$

Instead of the concept of slots per pole per phase in conventional rotor-PM machines, the spokes per phase in FSPM machines, q_{ph}, is defined as follows:

$$q_{ph} = N_s \cdot k_l/(2\tau \cdot m) \quad (5)$$

The electrical slot-pitch angle is given by,

$$\alpha_e = P_{aw} \cdot (2\pi/N_s) \quad (6)$$

while the angle between two adjacent spokes is given by,

$$\alpha_s = 2\pi/[N_s \cdot k_l/(2\tau)] \quad (7)$$

The winding factor, k_w, is expressed according to [28] as follows:

$$k_w = k_d \cdot k_p$$

$$k_d = \begin{cases} \sin\left(\frac{q_{ph}}{2} \cdot \frac{\alpha_s}{2}\right)/\left[\frac{q_{ph}}{2} \cdot \sin\left(\frac{\alpha_s}{2}\right)\right], & \text{if } q_{ph} \text{ is even} \\ \sin\left(q_{ph} \cdot \frac{\alpha_s}{4}\right)/\left[q_{ph} \cdot \sin\left(\frac{\alpha_s}{4}\right)\right], & \text{if } q_{ph} \text{ is odd} \end{cases}$$

$$k_p = \sin\left(\frac{y \cdot \alpha_e}{2}\right)$$

where, k_d is the distribution factor, k_p is the pitch factor, and y is the coil pitch, measured in number of slots.

The non-overlapping concentrated windings (NCWs) are preferable in conventional FSPM machines due to their short end turns. Nevertheless, the overlapping windings are also investigated in this paper.

SECTION A. Non-Overlapping Concentrated Windings

NCWs whose coil pitch is one ($y = 1$) include single-layer windings, double-layer windings, and multi-layer windings (here, these are represented by four-layer windings). These topologies will be analyzed and compared for a five-phase outer-rotor FSPM machine with 20/21 stator/rotor-pole as shown in Fig. 1(a), (b), and (c), respectively. In addition, a 10/21-p FSPM machine with double-layer winding is depicted in Fig. 1(d) for further stator/rotor-pole combination analysis. Their corresponding stars of slots are illustrated in Fig. 2(a), (b), (c), and (d), respectively.

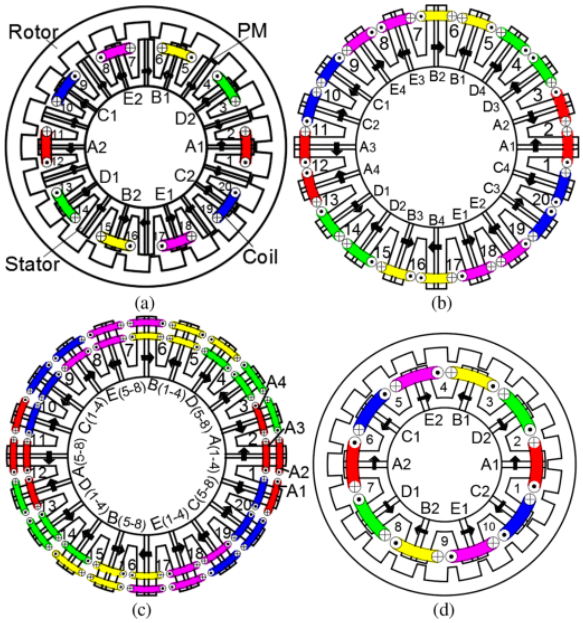

Fig. 1. (a) 20/21-p PSPM machine with single-layer winding. (b) Double-layer winding. (c) Four-layer winding. (d) 10/21-p FSPM machine with double-layer winding.

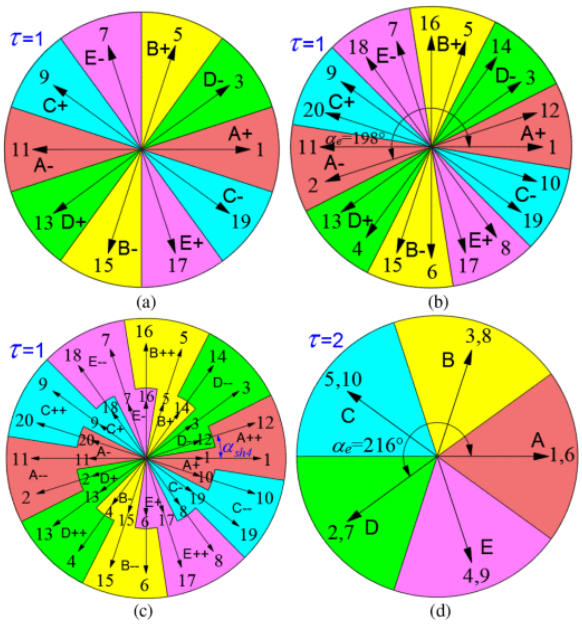

Fig. 2. Star of slots. (a) 20/21-p PSPM machine with single-layer winding. (b) Double-layer winding. (c) Four-layer winding. (d) 10/21-p FSPM machine with double-layer winding.

It is interesting to note that with introducing the concept of an armature winding pole-pair number, P_{aw}, into FSPM machines, though it is not equal to its magnet pair number as in regular rotor-PM motors, there is no need to take the polarity of coils into consideration when determining the winding connection. This method is quite different from, but much more convenient than that introduced in early works [29], [30]. For example, the two coils of phase A in 20/21-p machine with single-layer winding are in two different sectors, labeled *A+* and *A−* as shown in Fig. 2(a). Therefore, these coils should be in series-opposing connection as shown in Fig. 3(a), while those coils in a 10/21-p machine with double-layer winding are in the same sector, labeled *A* as shown in Fig. 2(d), and accordingly they are in series-aiding connection as shown in Fig. 3(b). This is coincident with those polarities depicted in Fig. 1(a) and (d), respectively.

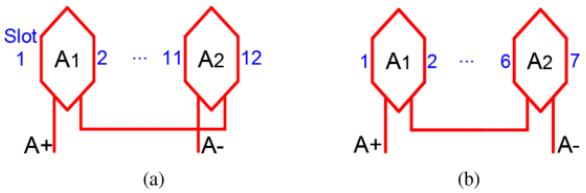

Fig. 3. Winding connection. (a) Series-opposing. (b) Series-aiding.

The back electromotive force (EMF) waveform of a single coil may be asymmetrical in FSPM machines due to the nature of the asymmetric magnetic flux paths as the rotor rotates. While, if the machine consists of one or more pairs of coils per phase whose magnetic flux paths having a phase shift of 180 electrical degrees, the even harmonics cancel each other and the phase back-EMF will be symmetrical [29]. Hence, for m-phase (m is odd) FSPM machines, there are two cases which can achieve symmetrical phase back-EMF waveform: (1) If q_{ph} is even, the number of rotor poles per basic repeating unit should be odd, and (2) If q_{ph} is odd, τ must be even, and the number of rotor poles for two basic repeating units should be odd. Thus, the condition for symmetrical phase back-EMF is summarized as follows:

$$\left.\begin{array}{c}(q_{ph}\text{ is even})\cap(N_s/\tau\text{ is odd})\\(q_{ph}\text{ is odd})\cap(\tau\text{ is odd})\cap(2N_s/\tau\text{ is odd})\end{array}\right\}\quad(11)$$

In single-layer winding machines, each slot is occupied by the coil side of a single phase [Fig. 1(a)]. The main winding parameters of five-phase single-layer winding FSPM machines with some feasible stator/rotor pole combinations are listed in Table I (# and * mean that the phase back-EMF waveform is asymmetrical for 10 stator-pole and 20 stator-pole machines, respectively). As can be seen, all of the phase back-EMF waveforms of the motors with 10 stator-poles are asymmetrical, while those machines with 20 stator-poles and odd rotor poles are symmetrical. In addition, when N_r is close to $(k \cdot N_s)$, e.g., 10/11-p, 10/21-p, 20/21-p, those machines exhibit a larger winding factor, resulting in higher torque density.

TABLE I Main Winding Parameters of Single-Layer Winding FSPM Machines

N_s	N_r	$6^{\#}$	$7^{\#}$	$8^{\#}$	$9^{\#}$	$11^{\#}$	$12^{\#}$	$13^{\#}$
10	P_{aw}	1	2	3	4	6	7	8
	τ	1	1	1	1	1	1	1
	q_{ph}	1	1	1	1	1	1	1
	k_d	1	1	1	1	1	1	1
	k_q	0.309	0.588	0.809	0.951	0.951	0.809	0.588
	k_w	0.309	0.588	0.809	0.951	0.951	0.809	0.588
20	P_{aw}	- 4	- 3	- 2	- 1	1	2	3
	τ	N/A	N/A	N/A	N/A	1	2	1
	q_{ph}	N/A	N/A	N/A	N/A	2	1	2
	k_d	N/A	N/A	N/A	N/A	1	1	1
	k_q	N/A	N/A	N/A	N/A	0.156	0.309	0.454
	k_w	N/A	N/A	N/A	N/A	0.156	0.309	0.454
N_s	N_r	$14^{\#,*}$	$16^{\#,*}$	$17^{\#,*}$	$18^{\#,*}$	$19^{\#,*}$	$21^{\#,*}$	$22^{\#,*}$
10	P_{aw}	9	11	12	13	14	16	17
	τ	1	1	1	1	1	1	1
	q_{ph}	1	1	1	1	1	1	1
	k_d	1	1	1	1	1	1	1
	k_q	0.309	0.309	0.588	0.809	0.951	0.951	0.809
	k_w	0.309	0.309	0.588	0.809	0.951	0.951	0.809
20	P_{aw}	4	6	7	8	9	11	12
	τ	2	2	1	2	1	1	2
	q_{ph}	1	1	2	1	2	2	1
	k_d	1	1	1	1	1	1	1
	k_q	0.588	0.809	0.891	0.951	0.988	0.988	0.951
	k_w	0.588	0.809	0.891	0.951	0.988	0.988	0.951

In double-layer winding machines, each slot is split equally for two coil sides from one or two phases [Fig. 1(b)]. The main winding parameters are listed in Table II. As can be seen, all machines with $q_{ph} \neq 2$ can achieve symmetrical phase back-EMF. Therefore, in terms of symmetrical phase back-EMF, the feasible stator/rotor-pole combinations for machines with double-layer winding are much more than those with single-layer winding.

TABLE II Main Winding Parameters of Double-Layer Winding Machines

N_s	N_r	$6^{\#}$	7	$8^{\#}$	9	11	$12^{\#,*}$	13
10	τ	1	2	1	2	2	1	2
	q_{ph}	2	1	2	1	1	2	1
	k_d	1	1	1	1	1	1	1
	k_q	0.309	0.588	0.809	0.951	0.951	0.809	0.588
	k_w	0.309	0.588	0.809	0.951	0.951	0.809	0.588
20	τ	N/A	N/A	N/A	N/A	1	2	1
	q_{ph}	N/A	N/A	N/A	N/A	4	2	4
	k_d	N/A	N/A	N/A	N/A	0.988	1	0.988
	k_q	N/A	N/A	N/A	N/A	0.156	0.309	0.454

	k_w	N/A	N/A	N/A	N/A	0.155	0.309	0.448
N_s	N_r	14[#,*]	16[#,*]	17	18[#]	19	21	22[#]
10	τ	1	1	2	1	2	2	1
	q_{ph}	2	2	1	2	1	1	2
	k_d	1	1	1	1	1	1	1
	k_q	0.309	0.309	0.588	0.809	0.951	0.951	0.809
	k_w	0.309	0.309	0.588	0.809	0.951	0.951	0.809
20	τ	4	2	1	4	1	1	4
	q_{ph}	1	5	4	1	4	4	1
	k_d	1	1	0.988	1	0.988	0.988	1
	k_q	0.588	0.809	0.891	0.951	0.988	0.988	0.951
	k_w	0.588	0.809	0.880	0.951	0.976	0.976	0.951

Multi-layer winding machines comprise more than two coil sides per slot, and accordingly, a four-layer winding is considered in this paper. Compared with the counterpart of the machine with double-layer winding, the sectors of the machine in the star of slots with four-layer winding are doubled. As shown in Fig. 2(c), each phase has two positive and two negative sectors, e.g., sector A+, A++, and A−, A−. The second set of sectors, A++ and A−, is shifted by an angle α_{sh4}, which is decided by the structure of the specific machine to obtain a maximum winding factor. Hence, the winding factor is computed based on that of the two-layer winding as,

$$k_{w4} = k_{w2} \cdot \cos\left(\alpha_{sh4}/2\right) \quad (12)$$

where, k_{w4} and k_{w2} are the four-layer and double-layer winding factor, respectively. The purpose of the multi-layer winding topology is to reduce both the sub- and super-stator MMF harmonics based on the advantage of spatial misalignment, so that the back-EMF waveform will be closer to sinusoidal. For instance, the back-EMF waveforms and their harmonic content of the 10/22-p FSPM machines with both double-layer and four-layer windings are shown in Fig. 4(a) and (b), respectively. The two machines have the same outer diameter, stack length, air-gap height, and number of turns per phase. As can be seen, the total harmonic distortion (THD) is significantly reduced from 17.17% with double-layer winding to 11.25% with four-layer winding, with a slight decrease of the fundamental component due to the winding factor given in eq. (12). This verified the previous analysis results. Moreover, it is interesting to note that, for 10 stator-pole machines with double-layer winding in Table II, the machines with odd number of rotor-poles can achieve symmetrical phase back-EMF, but suffer from UMF. By contrast, there is no UMF in even rotor-pole machines, but their phase back-EMFs are asymmetrical. Therefore, the four-layer winding concept offers good tradeoff between the back-EMF waveform and UMF for the 10 stator poles, even number rotor poles FSPM machines.

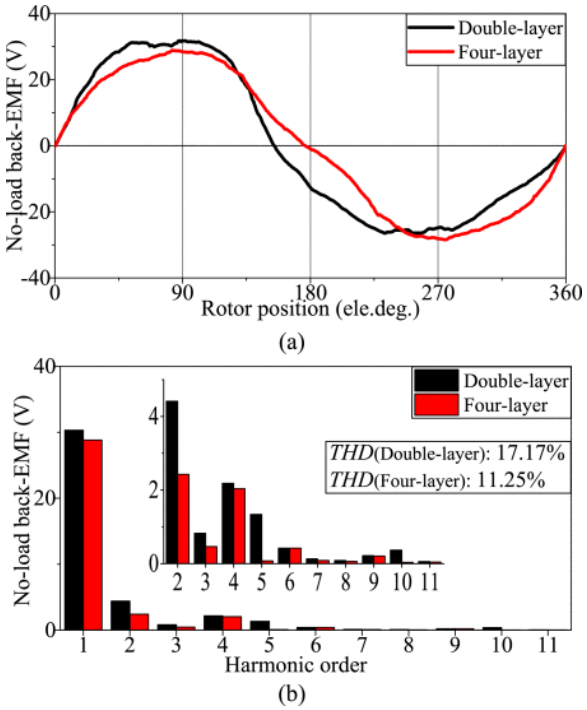

Fig. 4. Back-EMF of the 10/22-p FSPM machine. (a) Back EMF waveforms. (b) Harmonic spectrum.

B. Distributed Windings

The winding factor is an index of the goodness of the winding configuration, since it is proportional to the torque density. As can be observed in Table I and Table II, with NCWs, there are only a limited number of stator/rotor-pole combinations which can provide a relatively large winding factor, such as 10/11-p, 10/21-p, and 20/21-p. Furthermore, even with these combinations, the theoretical maximum value ($(k_w = 1)$) is unattainable unless $N_r = k \cdot N_s$, according to eq. (6) and eq. (10), which is infeasible due to the relationship in eq. (4). The main reason of low winding factors for the other combinations is the relatively low pitch factor, governed by eq. (10). Distributed windings can solve this problem.

In distributed winding machines, each coil is wound around more than one stator tooth, i.e., $y > 1$, thus the coils will overlap each other. In general, the full-pitched winding is selected due to their maximum pitch factor. Hence, a full-pitched distributed winding configuration is proposed and applied to a 20/31-p FSPM machine as shown in Fig. 5(b), while its counterpart with non-overlapping concentrated winding (single-layer) is shown in Fig. 5(a). Their corresponding stars of slots are illustrated in Fig. 6. Their main winding parameters are listed in Table III. The back-EMF waveforms and their harmonic content of the two motors are shown in Fig. 7(a) and (b), respectively. As can be seen, for the motor with non-overlapping concentrated winding, the pitch factor, k_q, is as low as 0.156, even though its distribution factor, k_d, is unit. While the winding factor of the motor with distributed winding is significantly improved from 0.156 to 0.988. In addition, by adopting a full-pitched distributed winding, the fundamental component of the back-EMF is increased by 6.31 times from 7.77 V to 49.02 V, which fairly matches the ratio between the winding factors of the two motors.

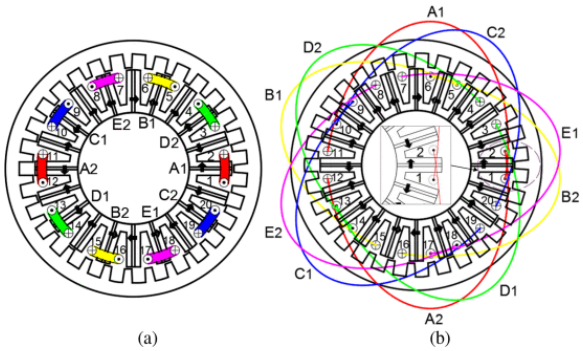

Fig. 5. Armature winding connection of the 20/31-p FSPM machine. (a) Conventional non-overlapping winding. (b) Distributed winding.

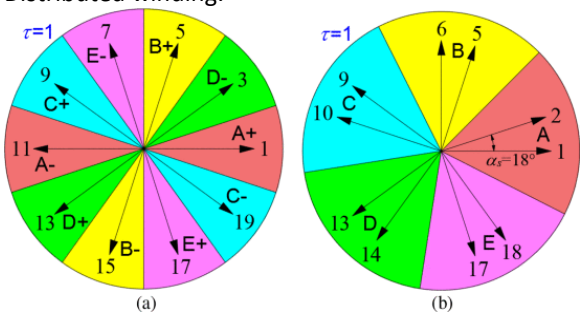

Fig. 6. Star of slots of the 20/31-p FSPM machine. (a) Conventional non-overlapping winding. (b) Distributed winding.

TABLE III Main Winding Parameters of the 20/31-p FSPM Machine

	t	q_{ph}	y	a_e	a_s	k_d	k_q	k_w
Concentrated	1	2	1	18	36	1	0.156	0.156
Distributed	1	2	10	18	18	0.988	1	0.988

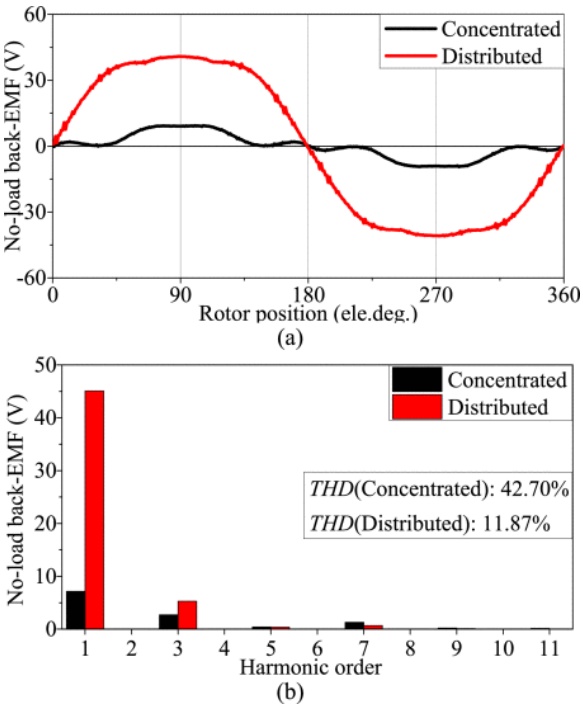

Fig. 7. Back-EMF of the 20/31-p FSPM machine. (a) Back EMF waveforms. (b) Harmonic spectra.

SECTION III. Comparison and Discussion

To comprehensively evaluate the performances of the five-phase outer-rotor FSPM machine with different winding configurations, four different winding topologies are selected and compared in this section, namely, 20/21-p machine with non-overlapping concentrated single-layer winding [Fig. 1(a)], double-layer winding [Fig. 1(b)], four-layer winding [Fig. 1(c)], and a 20/31-p machine with full-pitched distributed winding [Fig. 5(b)], respectively. For a fair comparison, some parameters of the four machines were kept the same as listed in Table IV. It should be noted that the rated electric frequencies are identical (217 Hz) for the four machines, thus, the rated speed is 620 r/min for the 20/21-p machines, while it is 420 r/min for the 20/31-p machine.

TABLE IV Parameters of the Four Investigated Machines

Parameter	Value	Parameter	Value
Rated phase current (A)	10	Stator inner radius (mm)	49
Rated frequency (Hz)	217	Stack length (mm)	85
Rotor outer radius (mm)	112.5	Number of turns /phase	96
Rotor inner radius (mm)	88.5	PM remanence NdfeB (T)	1.23
Air-gap length (mm)	0.5	PM volume (mm^3)	16500

A. Performance in Low-Speed Region

In low-speed region, motors in EV applications require good torque characteristics, average torque and overload capability, to provide enough acceleration, low cogging torque and torque ripple to reduce acoustic noise and vibration, high power factor and efficiency to save energy.

The flux density distribution of the four motors are depicted in Fig. 8(a), (b), (c), and (d), respectively. The open-circuit radial air-gap flux density profiles are shown in Fig. 9. It should be noted that for the three non-overlapping concentrated winding machines, the only difference is the winding configuration, therefore, the performances of the three machines under open-circuit condition are the same. It can be seen that in all cases, the air-gap flux density is non-sinusoidal and the peak values are as high as 2T in the vicinity of aligned stator and rotor poles due to the flux-concentration effect.

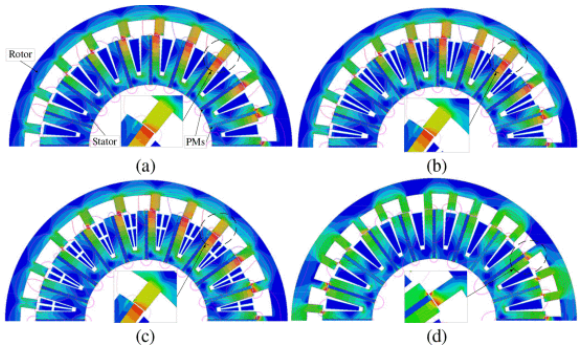

Fig. 8. Flux density distribution of the four motors. (a) 20/21-p machine with single-layer winding. (b) Double-layer winding. (c) Four-layer winding. (d) 20/31-p machine with distributed winding.

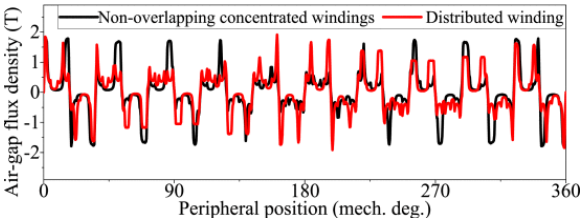

Fig. 9. Radial air-gap flux density.

The no-load back-EMF waveforms of the four machines and their harmonic spectra are shown in Fig. 10. As can be seen, all the four back-EMF waveforms are symmetrical. For the NCWs, although the back-EMF waveforms of the three machines are quite similar, the amplitudes of the harmonics and the THD are reduced from single to double to four-layer winding configurations. In addition, the fundamental component of the back-EMF of the machine with full-pitched distributed winding is the largest.

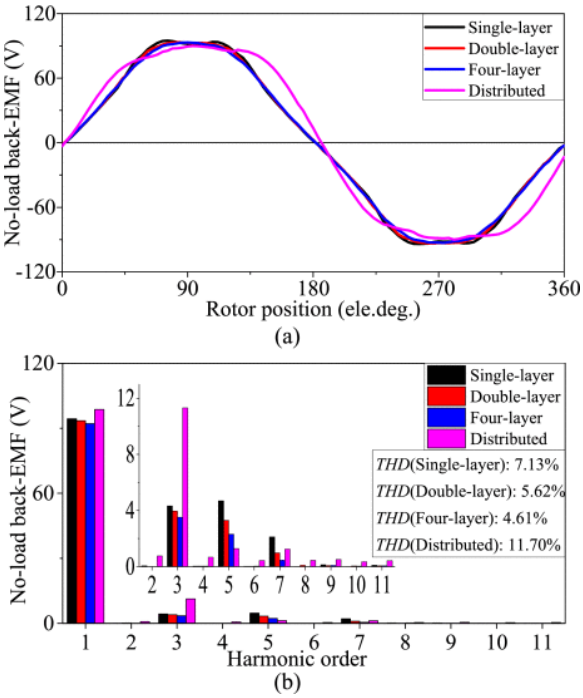

Fig. 10. No-load back-EMF (20/21-p @ 620 r/min, 20/31-p @ 420 r/min). (a) Back EMF waveforms. (b) Harmonic spectra.

Some main parameters at rated condition are summarized in Table V, where, ψ_m is the rms flux linkage due to the PMs, T_{cog} is the cogging torque, T_{avg} is the average torque, T_{ripple} is the torque ripple, P_f is the power factor, P_{cu} is the copper loss, P_{core} is the core loss, P_{PM} is the PM eddy-current loss, η is the efficiency. It was found that for the NCWs, a higher number of winding layers tends to reduce the sub- and super-harmonics, which reduces the torque ripple, core loss and PM eddy-current loss, therefore, improves the efficiency, with a little sacrifice of the PM flux linkage and average torque. Compared to the NCWs, the machine with distributed winding shows the largest PM flux linkage and average torque, but it possesses higher torque ripple and lower efficiency due to its rich stator MMF harmonics, moreover, its power factor is the lowest. In addition, the 20/21-p machines have a larger cogging torque than that of the 20/31-p one, because of the relationship between the cogging torque and the GCD of N_s and N_r [31].

TABLE V Performance of the Four FSPM Machines

	Single-layer	Double-layer	Four-layer	Distributed
Ψ_m(Wb)	0.0485	0.0480	0.0473	0.0541
T_{cog}(Nm)	0.52	0.52	0.52	0.32
T_{avg}(Nm)	50.22	49.89	49.26	66.96
T_{ripple}(%)	4.51	3.32	3.10	5.87
P_f	0.938	0.965	0.959	0.316
P_{cu}(W)	90.13	83.40	83.40	227.56
P_{core}(W)	118.09	112.59	108.28	227.30
P_{PM}(W)	85.23	82.09	80.77	164.00
η(%)	91.74	92.09	92.15	82.63

The overload capability is imperative for motors in EV applications, especially in hill-climbing and acceleration operations. Hence, the torque-current characteristics of the four machines are compared in Fig. 11. It shows that the variation of the torque versus current of the machines with double-layer and four-layer windings are almost the same, while they have better torque capability in the high *q*-axis current, i_q, region than that of the single-layer winding one. By contrast, the torque of the distributed winding machine is higher in the low i_q region, but much smaller in the high i_q region than that of its NCW counterparts. This can be explained by the torque equation given by,

$$T_{avg} = \frac{5}{2} N_r \psi_m i_q \quad (13)$$

View Source

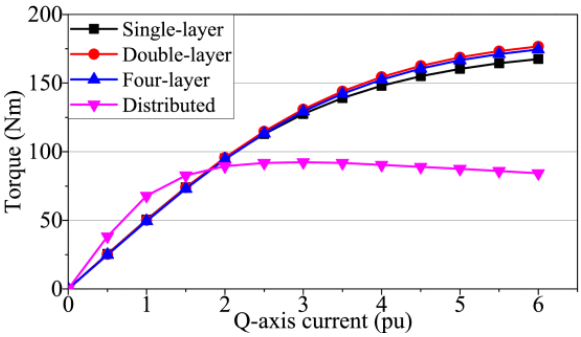

Fig. 11. Variation of torque versus current for the four machines.

There is no reluctance torque component because the difference between the *d*- and *q*-axis inductances is negligible which will be verified next. Therefore, all the four FSPM machines operate under zero *d*-axis current ($(i_d = 0)$) mode in this investigation. The PM flux linkage, ψ_m, is influenced by the i_q as shown in Fig. 12. It can be seen that with the i_q increasing, the PM flux linkage, ψ_m, of the distributed winding machine drops more sharply due to the more significant demagnetizing armature reaction effect caused by d- and q-axis cross-coupling, therefore, its torque saturates more quickly. However, the ψ_m of the NCW machines decreases slightly during the entire range, showing a stronger anti-saturation ability, and thus high overload capability.

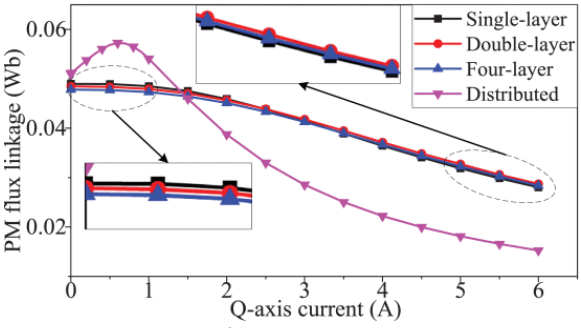

Fig. 12. D-axis PM flux linkage versus *q*-axis current.

B. Flux-Weakening Capability in High-Speed Region

For traction applications, the flux-weakening capability is of particular importance since it determines the loading capability and constant power speed range in the high-speed region. The flux weakening can be explained as follows:

Using Clarke and Park transformation, the five-phase quantities can be converted to two-phase, namely, d and q quantities as follows:

$$\begin{aligned} V_d &= Ri_d - \omega_e L_q i_q \\ V_q &= Ri_q + \omega_e(\psi_m + L_d i_d) \\ i_s^2 &= i_d^2 + i_q^2 \le i_{max}^2 \\ V^2 &= V_d^2 + V_q^2 \le V_{max}^2 \end{aligned}$$

where, V_d, V_q and L_d, L_q are the d- and q-axis voltages and inductances, R is the phase resistance, ω_e is the electrical angular frequency velocity, i_s is the rated stator phase current, V is the phase terminal voltage, i_{max} and V_{max} are the current and voltage limits. In principle, the terminal voltage, V, is almost proportional to the rotational speed below the base speed, n_b. As speed increases above n_b, the flux-weakening control mode should be implemented by adjusting the phase angle of i_s, and as a result, the ψ_m is reduced to some extent by the negative i_d, so that the voltage will be kept within its limit. Hence, the flux-weakening coefficient, k_{fw}, is defined to quantify the flux-weakening capability as follows:

$$k_{fw} = L_d i_s / \psi_m \quad (18)$$

Table VI reports the flux-weakening performance of the four machines. As can be seen, all saliency ratios ((L_q/L_d)) of the four machines are less than 1.2 *pu*, which is the reason why the reluctance toque is neglected in eq. (13). Moreover, the flux-weakening coefficients, k_{fw}, of the machines with double- and four-layer windings are smaller than that of the single-layer winding machine. This is due to their smaller L_d. It should be noted that the characteristic current, $I_{ch} = \psi_m/L_d$, of the machines with concentrated winding is higher than the rated current of 10 A and hence they have a cutoff speed/limited constant power speed range. While in case of the machine with distributed winding, the characteristic current, I_{ch}, is lower than the rated current and hence it has the capability to achieve a wide constant power range but at a reduced level proportional to the ratio of the machine characteristic current to the machine rated current [32], [33]. The torque and power versus speed at the limit voltage of the four machines are shown in Fig. 13. As can be seen, the machine with the distributed winding has the largest torque capability in the low-speed region if the rated current of 10A is applied, while it has the best flux-weakening capability in the high-speed region if the reduced current is applied. Hence, the distributed winding machine has better flexibility to operate throughout the entire speed range.

TABLE VI Flux-Weakening Performance of the Four FSPM Machines

	Single-layer	Double-layer	Four-layer	Distributed
n_b(r/min)	620	620	620	420
V_{max}(V)	75.80	72.86	72.37	225.22
L_d(mH)	2.01	1.61	1.68	15.65
L_q(mH)	2.32	1.87	1.94	15.79
L_q/L_d	1.154	1.161	1.155	1.009
k_{fw}	0.41	0.33	0.35	2.89

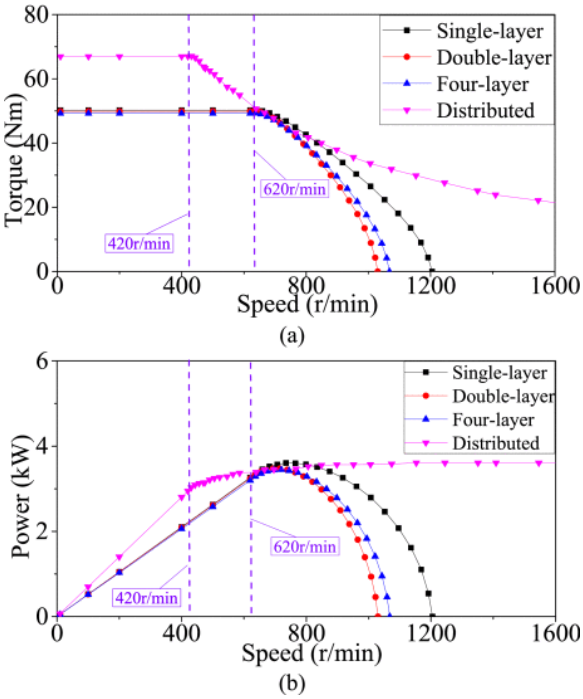

Fig. 13. Flux-weakening capability of the four motors. (a) Torque vs. speed. (b) Power vs. speed.

C. Fault-Tolerant Capability

Fault-tolerant technology is crucial for the post-fault continued operation of the motor, especially for safety-critical applications. Inductances are good indicators to quantify the fault-tolerant capability. Hence, the inductances of the four machines are listed in Table VII, where, L_{AA} is the self-inductance, L_{AB}, L_{AC}, L_{AD}, and L_{AE} are the mutual inductances which are presented as a percentage of L_{AA}. It shows that with the number of layers increasing in the NCW machines (single-layer, double-layer, and four-layer), the self-inductance decreases. While the distributed winding machine has both the largest self-inductance and mutual inductances, due to its largest permeance caused by its largest flux cross-sectional area and hence it has high flux linkage [21]. It is interesting to note that L_{AA} of the four-layer winding machine is smaller than that of its counterpart with double-layer winding, while its d-axis inductance, L_d, is larger, and therefore its flux-weakening capability is better, see Table VI. The reason is that the four-layer winding machine has larger mutual inductance.

TABLE VII Inductances of the Four FSPM Machines

Inductances	Single-layer	Double-layer	Four-layer	Distributed
L_{AA}(mH)	4.00	2.57	2.14	11.76
L_{AB}(¾)	1.75	0.39	0.47	5.36
L_{AC}(%)	10.5	5.06	20.09	30.95
L_{AD}(¾)	10.5	5.06	20.09	30.95
L_{AE}(%)	1.75	0.39	0.47	5.36

The profiles of the short-circuit currents in case of a terminal short circuit for the four machines are shown in Fig. 14. As can be seen, a high number of layers indicate larger short-circuit current amplitudes, while the short-circuit current of the distributed winding machine is the lowest in amplitude. This is consistent with the analysis results of inductances given earlier in Table VII.

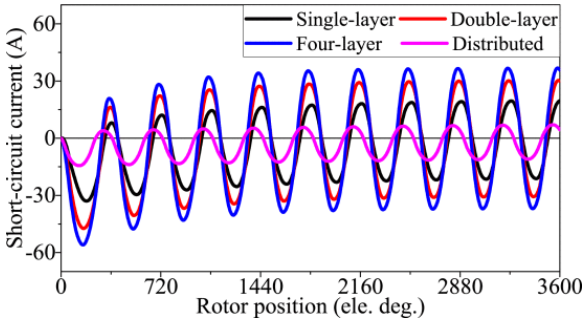

Fig. 14. Short-circuit currents versus the variation of the rotor position.

The performance of the four machines under open-circuit faults is investigated here in this paper, including one phase (Phase *A*), two adjacent phases (Phase *A* and Phase *B*), and two non-adjacent phases (Phase *A* and Phase *C*) open-circuit faults, respectively. In order to keep the stator MMF constant before and after an open-circuit fault occurs based on the fault-tolerant control strategy in [34], the healthy and post-fault current excitations (amplitude and phase angle) have to be readjusted as listed in Table VIII. The torque characteristics of the machines after implementation of the fault-tolerant control strategy are listed in Table IX, in which, the post-fault average torques, T_{avg}, as a percentage of the healthy value of T_{avg} are included within the parentheses. As can be seen, for the three NCW machines, a machine with a high number of winding layers exhibits closer average torque under fault to that in its healthy condition. For example, under Phase *A* and Phase *B* open-circuit faulty condition, the post-fault average torques are from 74.09% to 87.23% to 91.56% of their healthy average torques for the single-layer to the double-layer to the four-layer winding machines, respectively. In addition, a winding with a high number of layers effectively reduces the torque ripple under open-circuit faults. The distributed winding machine shows worse torque characteristics under fault due to its high self- and mutual inductances. Another reason could be that more serious saturation occurs due to the large post-fault currents. It should be noted that this study is mainly focused on outer-rotor FSPM machines. In order to provide a better understanding of how the winding configurations affect the various machine topologies, four inner-rotor FSPM machines with different winding configurations are also investigated as shown in the Appendix. As can be seen, similar conclusions are drawn as in the case of the outer-rotor FSPM machines.

TABLE VIII Current Excitations of the Machines Under Different Conditions

	Healthy	*A* open	*A&B* open	*A&C* open
A	(I, 0)	0	0	0
B	(I, -2π/5)	(1.382I, -π /5)	0	(1.382I, -2 π /5)
C	(I, -4π/5)	(1.382I, -4n /5)	(2.236I, -2 π /5)	0
D	(I, -6π/5)	(1.382I, 4 π /5)	(3.618I, 4 π /5)	(2.236I, - π)
E	(I, -8π/5)	(1.382I, π /5)	(2.236I, 0)	(2.236I, π /5)

TABLE IX Torque Characteristics of the Machines in Faulty Conditions

		Single-layer	Double-layer	Four-layer	Distributed
Healthy	T_{avg}(Nm)	50.22	49.89	49.26	66.96
	T_{ripple}(%)	4.51	3.32	3.10	5.87
A Open	T_{avg}(Nm)	48.95 (97.49%)	49.38 (98.98%)	48.82 (99.11%)	60.74 (90.71%)
	T_{ripple}(%)	15.92	12.29	11.41	45.21
A&B Open	T_{avg}(Nm)	37.21 (74.09%)	43.52 (87.23%)	45.10 (91.56%)	49.51 (73.94%)
	T_{ripple}(%)	67.41	34.60	27.17	74.73
A&C Open	T_{avg}(Nm)	45.54 (90.68%)	47.94 (96.09%)	47.96 (97.36%)	54.14 (80.85%)

	T_{ripple}(%)	34.03	18.22	17.02	53.15

SECTION IV. Experimental Validation

So far, the five-phase outer-rotor 10/21-p FSPM machine with E-core stator was manufactured and tested as shown in Fig. 15, while the 20/21-p NCW FSPM machine with different number of winding layers is still under construction. The advantages of the FSPM machine with an E-core stator over its counterpart with traditional U-core stator has been emphasized in [35] and [36].

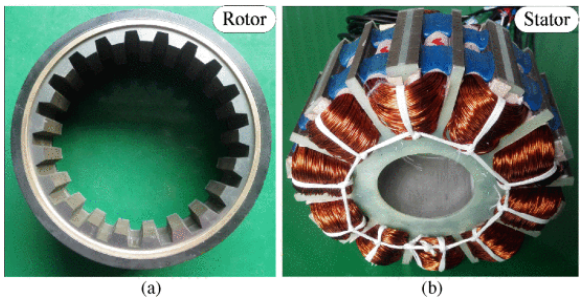

Fig. 15. Prototype of the Five-phase FSPM Machine. (a) Rotor. (b) Stator.

The phase back-EMF waveform and its harmonic spectra under open circuit condition at 200 r/min is shown in Fig. 16. As can be seen, the measured and finite element (FE) simulated back-EMF waveforms are in acceptable agreement, although the measured back-EMF is 8.25% lower than the 2-D FE-prediction due to end-effect and manufacturing imperfections. In addition, the calculated and measured phase resistance are 0.231 Ω and 0.239 Ω, respectively. They are also in good agreement. These measured results verify the accuracy and validity of the finite element modeling and simulation process presented in this paper.

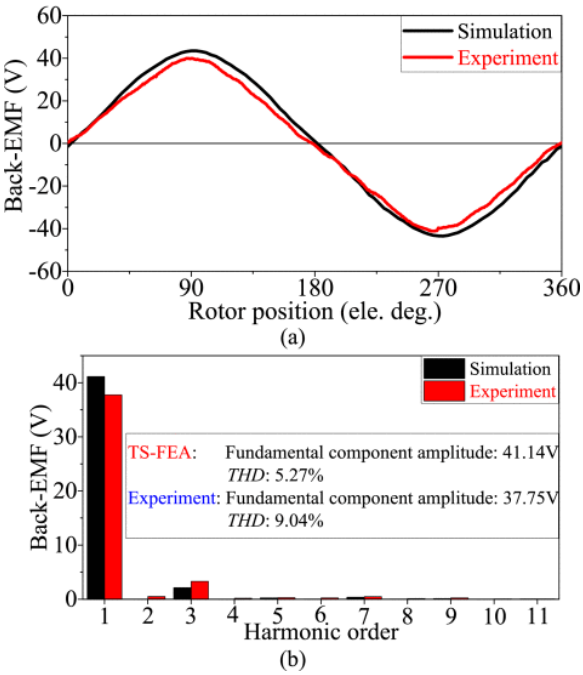

Fig. 16. (a) Predicted and measured back-EMF of the FSPM machine @ 200 r/min. (b) Harmonic spectra.

SECTION V. Conclusion

In this paper, a generic method for winding design of FSPM machines, associated with feasible number of stator/rotor-pole combinations was introduced. Hence, four five-phase outer-rotor FSPM machines with different winding configurations were modeled, investigated, and compared in detail, where various tradeoffs were discussed. Therefore, the following conclusions can be inferred from the results of this work:

With the presented winding design method, by introducing the concepts of armature winding pole-pair number based on the "magnetic gear effect", there is no need to take the polarity of coils into consideration when configuring the winding connection. It is much more convenient for designers than the methods already presented in the previous literature.

In NCW machines, there are only a limited number of stator/rotor-pole combinations which can provide a relatively large winding factor. Meanwhile, a distributed winding approach can solve this low winding factor problem. A full-pitched distributed winding FSPM machine provides significant improvement regarding winding factor values and the magnitude of the fundamental component of the back-EMF, compared with its counterpart with non-overlapping winding.

In NCW machines, with the number of winding layers increasing, the machine exhibits better back-EMF waveform, less torque ripple and lower losses, higher efficiency, and better fault-tolerant capability under open-circuit faults, but less average torque, less self-inductance and therefore larger short-circuit currents.

Among the four machines compared in Section III of this paper, the double-layer winding machine exhibits the highest power factor and the best overload capability. The four-layer winding machine provides the lowest torque ripple, lowest losses and therefore highest efficiency. Meanwhile, the distributed winding machine has the largest average torque, best flux-weakening capability, and lowest short-circuit current, but highest losses and therefore lowest efficiency, worst overload capability and worst fault-tolerant capability under open-circuit faults. Accordingly, the appropriate tradeoffs should be made when designing/choosing the winding configurations suitable to the specific application under consideration.

ACKNOWLEDGMENT

The authors would like to express sincere thanks to ANSYS, Inc. for the software support.

Appendix A Case Study of Inner-Rotor FSPM Machines

The main parameters of the four investigated inner-rotor FSPM machines are listed in Table X. It should be noted that the inner-rotor machines and the out-rotor machines have the same physical air-gap (from 88 mm to 88.5 mm). This is because in this way, the inner-rotor machines and the outer-rotor machines can be cut and flatten to be the same linear machines.

TABLE X Parameters of the Four Investigated Inner-Rotor Machines

Parameter	Value	Parameter	Value
Rated phase current (A)	10	Rotor inner radius (mm)	64
Rated frequency (Hz)	217	Stack length (mm)	85
Stator outer radius (mm)	127.5	Number of turns/phase	96
Stator inner radius (mm)	88.5	PM remanence NdFeB (T)	1.23
Air-gap length (mm)	0.5	PM volume (mm^3)	16500

The flux density distribution of the four inner-rotor motors are depicted in Fig. 17. The no-load back-EMF waveforms of the four inner-rotor FSPM machines and their harmonic spectra are shown in Fig. 18. As can be

seen, for the NCW machines, the amplitude of the fundamental harmonic component and the THD are reduced from single to double to four-layer winding configurations. The fundamental component of the back-EMF of the distributed winding machine is the highest. Some main parameters of the four inner-rotor machines at rated condition are listed in Table XI. It was found that for the NCWs, a higher number of winding layers tends to reduce the torque ripple, core loss, and PM eddy-current loss, and therefore, improve the efficiency, with a little sacrifice of the PM flux linkage and average torque. While the distributed winding machine shows the largest PM flux linkage and average torque, but it possesses higher torque ripple and lower efficiency. The torque-current characteristics of the four inner-rotor machines showing the overload capability are depicted in Fig. 19. These results of the inner-rotor FSPM machines are consistent with those of the outer-rotor FSPM machines.

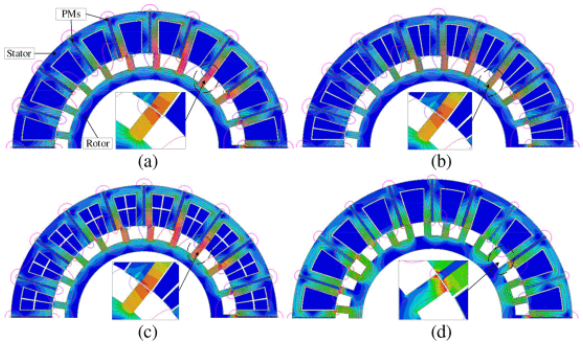

Fig. 17. Flux density distribution of the four inner-rotor motors. (a) 20/21-p machine with single-layer winding. (b) Double-layer winding. (c) Four-layer winding. (d) 20/31-p machine with distributed winding.

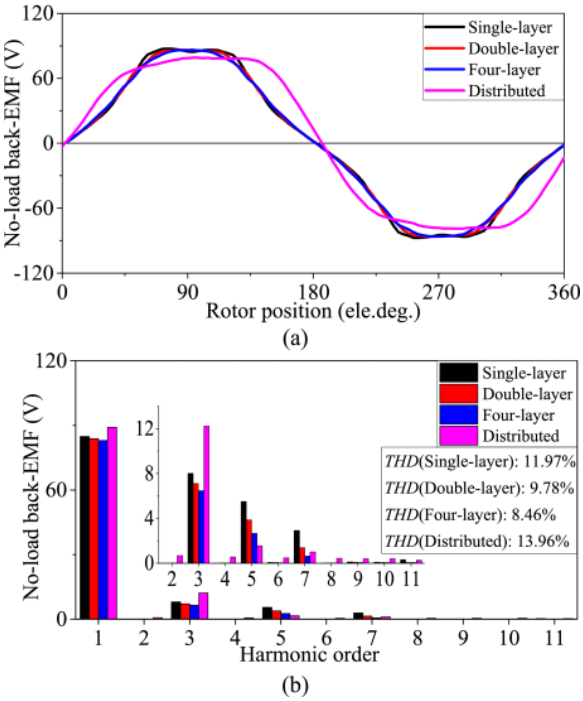

Fig. 18. No-load back-EMF of the four inner-rotor machines (20/21-p @ 620 r/min, 20/31-p @ 420 r/min). (a) Back EMF waveforms. (b) Harmonic spectra.

TABLE XI Performance of the Four Inner-Rotor FSPM Machines

	Single-layer	Double-layer	Four-layer	Distributed
ψ_m(Wb)	0.0437	0.0430	0.0426	0.0486
T_{cog}(Nm)	1.02	1.02	1.02	0.75

T_{avg}(Nm)	45.19	44.85	44.36	58.83
T_{ripple}(%)	3.98	3.48	2.77	3.95
P_f	0.938	0.967	0.970	0.350
P_{cu}(W)	97.92	89.04	89.04	431.11
P_{core}(W)	116.13	110.83	105.79	247.79
P_{PM}(W)	86.96	83.06	82.29	182.40
17(%)	90.69	91.14	91.20	75.02

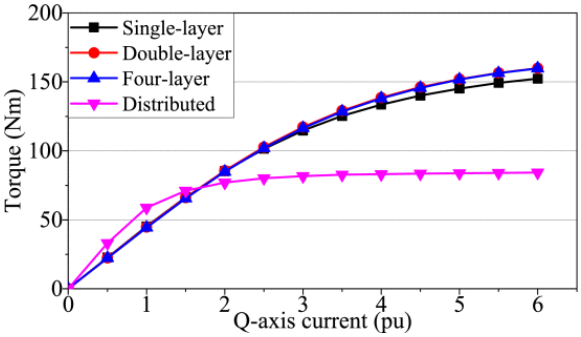

Fig. 19. Variation of torque versus current for the four inner-rotor machines.

The flux-weakening performance parameters of the four inner-rotor machines are listed in Table XII. The torque and power versus speed at the limited voltage of the four machines are shown in Fig. 20(a) and (b), respectively. As can be seen, for the NCWs, a higher number of winding layers indicates lower *d*-axis inductance, and therefore, worse flux-weakening capability. By contrast, the distributed winding machine has the largest torque capability in the low-speed region if the rated current of 10 A is applied, while it has the best flux-weakening capability in the high-speed region if the reduced current is applied. These results of the inner-rotor FSPM machines are similar to those of the out-rotor FSPM machines.

TABLE XII Flux-Weakening Parameters of the Four Inner-Rotor Machines

	Single-layer	Double-layer	Four-layer	Distributed
n_b(r/min)	620	620	620	420
V_{max}(V)	68.94	66.07	65.19	197.12
L_d(mH)	1.96	1.61	1.55	13.54
L_q(mH)	2.25	1.86	1.80	13.74
L_q/L_d	1.148	1.155	1.161	1.015
k_{fw}	0.45	0.37	0.36	2.79

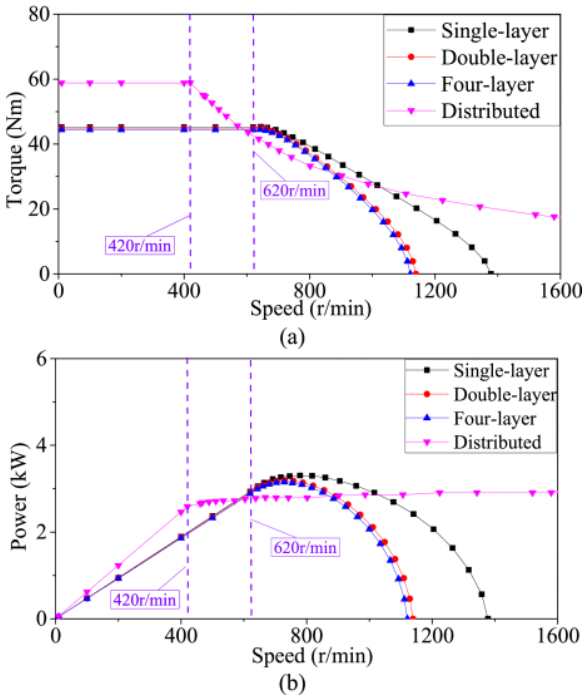

Fig. 20. Flux-weakening capability of the four inner-rotor machines. (a) Torque vs. speed. (b) Power vs. speed.

The inductances of the four inner-rotor machines are listed in Table XIII. The profiles of the short-circuit currents in case of a terminal short circuit for the four inner-rotor machines are depicted in Fig. 21. The torque characteristics of the machines after implementation of the fault-tolerant control strategy (see Table VIII) are listed in Table XIV. As can be seen, with the number of winding layers increasing in the NCW machines (from single-layer to double-layer to four-layer), the self-inductance decreases, the short-circuit current increases, the average torque under open-circuit faults is closer to that in its healthy condition, the torque ripple under open-circuit faults reduces. By contrast, the distributed winding machine has the largest self-inductance, the lowest short-circuit current, and the worst torque characteristics under open-circuit faults. These results of the inner-rotor machines are also consistent with those of the out-rotor FSPM machines.

TABLE XIII Inductances of the Four Inner-Rotor FSPM Machines

Inductances	Single-layer	Double-layer	Four-layer	Distributed
L_{AA}(mH)	3.67	2.39	1.89	10.81
L_{AB}(%)	1.85	0.39	0.08	3.70
L_{AC}(%)	10.35	5.08	20.25	27.02
L_{AD}(%)	10.35	5.08	20.25	27.01
L_{AE}(%)	1.85	0.39	0.08	3.70

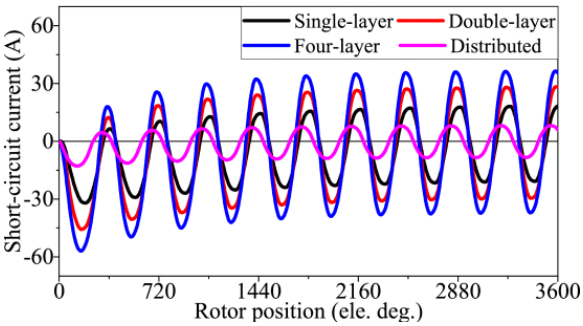

Fig. 21. Short-circuit currents versus the variation of the rotor position for the four inner-rotor machines.

TABLE XIV Torque Characteristics of the Four Inner-Rotor Machines In Faulty Conditions

		Single-layer	Double-layer	Four-layer	Distributed
Healthy	T_{avg}(Nm)	45.19	44.85	44.36	58.83
	T_{ripple}(%)	3.98	3.48	2.77	3.95
A Open	T_{avg}(Nm)	44.02 (97.41%)	44.39 (98.97%)	44.02 (99.23%)	52.54 (89.31%)
	T_{ripple}(%)	21.23	18.10	16.81	49.51
A&B Open	T_{avg}(Nm)	33.45 (74.02%)	39.00 (86.96%)	40.71 (91.77%)	41.46 (70.47%)
	T_{ripple}(%)	74.58	44.10	36.54	87.81
A&C Open	T_{avg}(Nm)	41.06 (90.86%)	43.13 (96.16%)	43.29 (97.59%)	45.30 (77.00%)
	T_{ripple}(%)	51.34	31.23	28.57	62.03

References

1. J. H. Kim, I. O. Lee, G. W. Moon, "Analysis and design of a hybrid-type converter for optimal conversion efficiency in electric vehicle chargers", *IEEE Trans. Ind. Electron.*, vol. 64, no. 4, pp. 2789-2800, Apr. 2017.

2. F. Lu, H. Zhang, H. Hofmann, C. C. Mi, "A dynamic charging system with reduced output power pulsation for electric vehicles", *IEEE Trans. Ind. Electron.*, vol. 63, no. 10, pp. 6580-6590, Oct. 2016.

3. A. Dadashnialehi, A. Bab-Hadiashar, Z. Cao, A. Kapoor, "Intelligent sensorless antilock braking system for brushless in-wheel electric vehicles", *IEEE Trans. Ind. Electron.*, vol. 62, no. 3, pp. 1629-1638, Mar. 2015.

4. M. Cheng, W. Hua, J. Zhang, W. Zhao, "Overview of stator-permanent magnet brushless machines", *IEEE Trans. Ind. Electron.*, vol. 58, no. 11, pp. 5087-5101, Nov. 2011.

5. K. T. Chau, C. C. Chan, C. Liu, "Overview of permanent-magnet brushless drives for electric and hybrid electric vehicles", *IEEE Trans. Ind. Electron.*, vol. 55, no. 6, pp. 2246-2257, Jun. 2008.

6. X. Cai, M. Cheng, S. Zhu, J. Zhang, "Thermal modeling of flux-switching permanent-magnet machines considering anisotropic conductivity and thermal contact resistance", *IEEE Trans. Ind. Electron.*, vol. 63, no. 6, pp. 3355-3365, Jun. 2016.

7. H. Hua, Z. Q. Zhu, "Novel partitioned stator hybrid excited switched flux machines", *IEEE Trans. Energy Convers.*, vol. 32, no. 2, pp. 495-504, Jun. 2017.

8. Z. Z. Wu, Z. Q. Zhu, "Analysis of magnetic gearing effect in partitioned stator switched flux PM machines", *IEEE Trans. Energy Convers.*, vol. 31, no. 4, pp. 1239-1249, Dec. 2016.

9. Z. Q. Zhu, J. T. Chen, Y. Pang, D. Howe, S. Iwasaki, R. Deodhar, "Analysis of a novel multi-tooth flux-switching PM brushless AC machine for high torque direct-drive applications", *IEEE Trans. Magn.*, vol. 44, no. 11, pp. 4313-4316, Nov. 2008.

10. L. Parsa, H. A. Toliyat, "Five-phase permanent-magnet motor drives", *IEEE Trans. Ind. Appl.*, vol. 41, no. 1, pp. 30-37, Jan. 2005.

11. E. B. Sedrine, J. Ojeda, M. Gabsi, I. Slama-Belkhodja, "Fault-tolerant control using the GA optimization considering the reluctance torque of a five-phase flux switching machine", *IEEE Trans. Energy Convers.*, vol. 30, no. 3, pp. 927-938, Sep. 2015.

12. X. Zhu, Z. Shu, L. Quan, Z. Xiang, X. Pan, "Design and multicondition comparison of two outer-rotor flux-switching permanent-magnet motors for in-wheel traction applications", *IEEE Trans. Ind. Electron.*, vol. 64, no. 8, pp. 6137-6148, Aug. 2017.

13. E. Hoang, H. B. Ahmed, J. Lucidarme, "Switching flux permanent magnet polyphased synchronous machines", *Proc. Eur. Conf. Power Electron. Appl.*, pp. 3903-3908, Sep. 1997.

14. A. M. EL-Refaie, "Fractional-slot concentrated-windings synchronous permanent magnet machines: Opportunities and challenges", *IEEE Trans. Ind. Electron.*, vol. 57, no. 1, pp. 107-121, Jan. 2010.

15. L. Alberti, N. Bianchi, "Theory and design of fractional-slot multilayer windings", *IEEE Trans. Ind. Appl.*, vol. 49, no. 2, pp. 841-849, Mar. 2013.

16. P. B. Reddy, A. M. EL-Refaie, K. K. Huh, "Effect of number of layers on performance of fractional-slot concentrated-windings interior permanent magnet machines", *IEEE Trans. Power Electron.*, vol. 30, no. 4, pp. 2205-2218, Apr. 2015.

17. Y. Wang, R. Qu, J. Li, "Multilayer windings effect on interior PM machines for EV applications", *IEEE Trans. Ind. Appl.*, vol. 51, no. 3, pp. 2208-2215, May 2015.

18. C. C. Hwang, C. M. Chang, S. S. Hung, C. T. Liu, "Design of high performance flux switching PM machines with concentrated windings", *IEEE Trans. Magn.*, vol. 50, no. 1, Jan. 2014.

19. Z. Wang, W. Xu, G. Lei, J. Zhu, "Multilayer winding effect on performance of flux-switching permanent magnet machines", *IEEE Trans. Appl. Supercond.*, vol. 26, no. 7, Oct. 2016.

20. D. Li, R. Qu, J. Li, W. Xu, L. Wu, "Synthesis of flux switching permanent magnet machines", *IEEE Trans. Energy Convers.*, vol. 31, no. 1, pp. 106-117, Mar. 2016.

21. L. Shao, W. Hua, Z. Q. Zhu, X. Zhu, M. Cheng, Z. Wu, "A novel flux-switching permanent magnet machine with overlapping windings", *IEEE Trans. Energy Convers.*, vol. 32, no. 1, pp. 172-183, Mar. 2017.

22. Y. Du, C. Zou, X. Zhu, C. Zhang, F. Xiao, "A full-pitched flux-switching permanent-magnet motor", *IEEE Trans. Appl. Supercond.*, vol. 26, no. 4, Jun. 2016.

23. Y. Du et al., "Comparison of flux-switching PM motors with different winding configurations using magnetic gearing principle", *IEEE Trans. Magn.*, vol. 52, no. 5, May 2016.

24. W. Hua, P. Su, M. Tong, J. Meng, "Investigation of a five-phase E-core hybrid-excitation flux-switching machine for EV and HEV applications", *IEEE Trans. Ind. Appl.*, vol. 53, no. 1, pp. 124-133, Jan. 2017.

25. Y. Tang, J. J. H. Paulides, E. A. Lomonova, "Topologies of flux-switching machines for in-wheel traction", *Proc. 8th Int. Conf. Exhib. Ecol. Veh. Renewable Energies*, pp. 1-6, 2013.

26. J. Wang, W. Wang, K. Atallah, D. Howe, "Design considerations for tubular flux-switching permanent magnet machines", *IEEE Trans. Magn.*, vol. 44, no. 11, pp. 4026-4032, Nov. 2008.

27. Y. Shi, L. Jian, J. Wei, Z. Shao, W. Li, C. C. Chan, "A new perspective on the operating principle of flux-switching permanent-magnet machines", *IEEE Trans. Ind. Electron.*, vol. 63, no. 3, pp. 1425-1437, Mar. 2016.

28. N. Bianchi, Power Electronics and Motor Drives, Boca Raton, FL, USA:CRC Press, pp. 6-22–6-26, 2011.

29. J. T. Chen, Z. Q. Zhu, "Winding configurations and optimal stator and rotor pole combination of flux-switching PM brushless AC machines", *IEEE Trans. Energy Convers.*, vol. 25, no. 2, pp. 293-302, Jun. 2010.

30. J. T. Chen, Z. Q. Zhu, "Comparison of all- and alternate-poles-wound flux-switching PM machines having different stator and rotor pole numbers", *IEEE Trans. Ind. Appl.*, vol. 46, no. 4, pp. 1406-1415, Jul. 2010.

31. N. Bianchi, S. Bolognani, "Design techniques for reducing the cogging torque in surface-mounted PM motors", *IEEE Trans. Ind. Appl.*, vol. 38, no. 5, pp. 1259-1265, Sep. 2002.

32. W. L. Soong, S. Han, T. M. Jahns, "Design of interior PM machines for field-weakening applications", *Proc. Int. Conf. Elect. Mach. Syst.*, pp. 654-664, 2007.

33. W. L. Soong, P. B. Reddy, A. M. El-Refaie, T. M. Jahns, N. Ertugrul, "Surface PM machine parameter selection for wide field-weakening applications", *Proc IEEE Ind. Appl. Annu. Meeting*, pp. 882-889, 2007.

34. S. Ding, W. Chen, M. Tong, F. Xie, C. Zheng, "Fault tolerant control for a five-phase permanent magnet synchronous machine driving system", *Proc. IEEE 11th Conf. Ind. Electron. Appl.*, pp. 2021-2025, 2016.

35. J. T. Chen, Z. Q. Zhu, S. Iwasaki, R. P. Deodhar, "A novel E-core switched-flux PM brushless AC machine", *IEEE Trans. Ind. Appl.*, vol. 47, no. 3, pp. 1273-1282, May 2011.

36. T. Raminosoa, C. Gerada, M. Galea, "Design considerations for a fault-tolerant flux-switching permanent-magnet machine", *IEEE Trans. Ind. Electron.*, vol. 58, no. 7, pp. 2818-2825, Jul. 2011.